




Enzyme-induced mineralization of hydrogels with amorphous calcium carbonate for fast synthesis of ultrastiff, strong and tough organic–inorganic double networks

Marko Milovanovic¹, Lydia Mihailowitsch¹, Mathusiha Santhirasegaran¹, Volker Brandt¹, and Joerg C. Tiller^{1,*} 

¹Biomaterials and Polymer Science, Department of Bio- and Chemical Engineering, TU Dortmund, Emil-Figge-Str. 66, 44227 Dortmund, Germany

Received: 8 April 2021

Accepted: 24 May 2021

Published online:

23 June 2021

© The Author(s) 2021

ABSTRACT

Hydrogels with good mechanical properties have great importance in biological and medical applications. Double-network (DN) hydrogels were found to be very tough materials. If one of the two network phases is an inorganic material, the DN hydrogels also become very stiff without losing their toughness. So far, the only example of such an organic–inorganic DN hydrogel is based on calcium phosphate, which takes about a week to be formed as an amorphous inorganic phase by enzyme-induced mineralization. An alternative organic–inorganic DN hydrogel, based on amorphous CaCO₃, which can be formed as inorganic phase within hours, was designed in this study. The precipitation of CaCO₃ within a hydrogel was induced by urease and a urea/CaCl₂ calcification medium. The amorphous character of the CaCO₃ was retained by using the previously reported crystallization inhibiting effects of *N*-(phosphonomethyl)glycine (PMGly). The connection between organic and inorganic phases via reversible bonds was realized by the introduction of ionic groups. The best results were obtained by copolymerization of acrylamide (AAm) and sodium acrylate (SA), which led to water-swollen organic–inorganic DN hydrogels with a high Young's modulus (455 ± 80 MPa), remarkable tensile strength (3.4 ± 0.7 MPa) and fracture toughness (1.1 ± 0.2 kJ m⁻²).

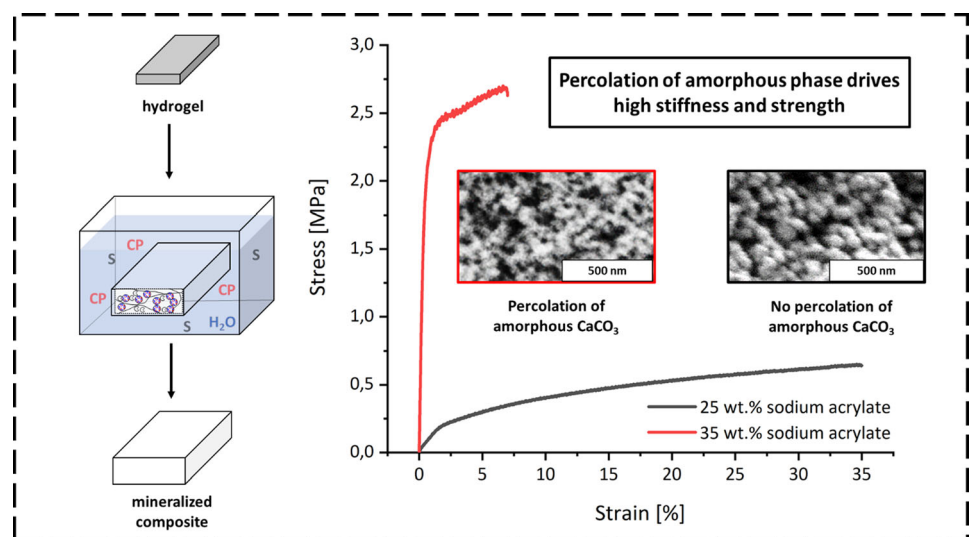
Handling Editor: Jaime Grunlan.

Address correspondence to E-mail: joerg.tiller@tu-dortmund.de

E-mail Addresses: marko.milovanovic@tu-dortmund.de; lydia.mihailowitsch@tu-dortmund.de; mathusiha.santhirasegaran@tu-dortmund.de; volker.brandt@tu-dortmund.de

GRAPHICAL ABSTRACT

The present manuscript describes the method of enzymatic mineralization of hydrogels for the production of ultrastiff and strong composite hydrogels. By forming a double-network structure based on an organic and an inorganic phase, it is possible to improve the mechanical properties of a hydrogel, such as stiffness and strength, by several orders of magnitude. The key to this is the formation of a percolating, amorphous inorganic phase, which is achieved by inhibiting crystallization of precipitated amorphous CaCO_3 with N-(phosphonomethyl)glycine and controlling the nanostructure with co polymerized sodium acrylate. This creates ultrastiff, strong and tough organic–inorganic double-network hydrogels.



Introduction

The development and synthesis of hydrogels with good mechanical properties are of high relevance to many research areas, such as biomaterials, tissue engineering [1, 2] and regenerative medicine [3–5], soft actuators [6, 7] and smart materials [8, 9], flexible electronics [10, 11], membranes [12–14], ion exchange materials [15] and many more. In addition to fiber-reinforced materials [16], nanocomposite hydrogels [17], dual cross-linked networks [18], amphiphilic polymer conetworks (APCNs) [19–25] and other diverse hydrogel-reinforcing mechanisms [26], double-network (DN) hydrogels have recently received increasing attention for improving the mechanical

properties of hydrogels [27–30]. DN hydrogels are composed of two hydrophilic networks that form interpenetrating structures through a two-step polymerization. Thereby, one of these polymer networks is higher cross-linked and usually synthesized first, while the second, loosely cross-linked and highly stretchable network is formed within the first network structure [28]. The interactions between the two polymer networks are based on sacrificial, reversible bonds, such as ionic bond, hydrogen bridges, or π – π stacking, and yield their high toughness. In contrast, the increase of the Young's modulus is limited to the naturally weak binding strength, particularly in aqueous environment.

Exchanging one of the organic networks in a DN hydrogel with an inorganic network can improve the

mechanical properties and create stiff hydrogels [31–33]. Numerous approaches of adding inorganic material to hydrogels have been described so far, for example, by adding inorganic fillers to the monomer solution [34–40], by adding silanes to the monomer solution [41–43] or the first network [42–45] or by forming an inorganic phase within the first hydrogel [33, 46]. The best improvement in stiffness has been achieved, if a percolated inorganic phase is formed within the hydrogel [33].

Recently, we reported on the enzymatic mineralization of hydrogels with alkaline phosphatase, creating a percolating organic/inorganic DN hydrogel with Young's moduli increased by several orders of magnitude, while increasing the strength of the composite [33]. This improvement in mechanical performance is due to the percolation of the amorphous inorganic nanostructures, which form a second network in the hydrogel matrix. According to our hypothesis, the best mechanical properties of an organic–inorganic DN hydrogel are achieved near the percolation point of the inorganic phase, where the latter yields the stiffness of the material, while the organic phase contributes to the toughness. Thus, the inorganic network needs to be isotropic and near the percolation point for the best-performing properties. Below this percolation point, there is no significant advantage in stiffness, while beyond, the inorganic network makes the hydrogel increasingly brittle. In principle, this should be working with every inorganic material. In order to generalize the concept, amorphous calcium carbonate (ACC) is considered as an alternative to amorphous calcium phosphate as an inorganic phase.

Although the previously described urease-induced precipitation of calcium carbonate generates water-swollen and highly mineralized hydrogel composites much faster than the alkaline phosphatase-induced mineralization [32], the resulting materials are brittle, which is due to crystallization and inhomogeneous growth of the inorganic phase [31, 33]. Recently, we described a method to inhibit the crystallization of CaCO_3 during the urease-induced precipitation in hydrogels with *N*-(phosphonomethyl)glycine (PMGly) as a solution additive. This led to homogeneous precipitation of spherical agglomerates of long-term stable amorphous CaCO_3 (ACC) in high quantity inside the hydrogel matrix. Although the urease-induced calcification leads to a uniform and homogenous precipitation of inorganic material

inside the hydrogel, no significant improvement of the mechanical properties was observed, which might be due to missing binding between polymer matrix and the precipitated inorganic material [47].

The goal of this work is to tailor the composition of the polymer matrix and the precipitation conditions to afford a percolated amorphous CaCO_3 matrix within the hydrogel that is connected with the latter via secondary, reversible bonds.

Experimental section

Materials

N,N-dimethyl acrylamide (DMA) with a purity of 99% was obtained from Merck. The monomer was distilled, stored at $-25\text{ }^\circ\text{C}$ under an argon atmosphere, and used within the next two weeks. Acrylamide (AAm) with a purity of 99%, sodium acrylate (SA) with a purity of 97% and triethylene glycol dimethacrylate (TEG) with 95% purity were obtained from Merck. *N,N*-methylene bis acrylamide (MBAm) of 99% purity was supplied by Merck. Acrylic acid (AA) with a purity of 99% was obtained from Merck and freshly distilled and stored under inert atmosphere at $-25\text{ }^\circ\text{C}$. Ethyl 2-[4-(dihydroxyphosphoryl)-2-oxabutyl] acrylate (EDPOA) was kindly provided by Ivoclar Vivadent GmbH. [2-(methacryloyloxy)ethyl]dimethyl-(3-sulfopropyl)ammonium hydroxide (DMAPS) with a purity of 98% and 2-Acrylamido-2-methylpropane sulfonic acid (AMPS) as a 50 wt.% aqueous solution were supplied by Merck. [2-(methacryloyloxy) ethyl] trimethylammonium chloride (QuAAc) solution (72 wt.% in H_2O) was purchased from VWR. 3-Sulfopropyl acrylate potassium (SPA) salt was purchased from Merck. The photoinitiator Irgacure 2959 was supplied by TCI Europe. Irgacure 651 was kindly provided by Ciba Specialty Chemicals (part of BASF). Urease from *Canavalia ensiformis* (Nr. 94,282) with an activity of 35 U/g was purchased from Merck and stored at $-25\text{ }^\circ\text{C}$. The urease formulation contains 10 wt.% of protein. Urea and calcium chloride were obtained from Merck and Alfa Aesar, and *N*-(phosphonomethyl)glycine was provided by Glentham Life Sciences, respectively. Triethanolamine (TEA) was from Merck. A 32 wt.% solution of HCl was from VWR. All chemicals were of analytical grade or purer

and used without further purification if not noted otherwise.

Preparation of TEA buffer

A 0.2 M TEA buffer (29.84 g TEA dissolved in 1000 mL bi-distilled and degassed water) was adjusted to a pH of 7.5 using a 1 M aqueous HCl solution and stored under argon atmosphere at room temperature.

Preparation of calcification solution

The different calcification solutions were prepared by dissolving 1 g l^{-1} *N*-(phosphonomethyl)-glycine and varying amounts of CaCl_2 and urea in 900 ml of the TEA buffer (typically 30 g l^{-1} CaCl_2 , 10 g l^{-1} urea and 1 g l^{-1} PMGly). Then, the TEA buffer was added to fill the solution up to 1000 ml (final concentrations: 30 g l^{-1} CaCl_2 , 10 g l^{-1} urea and 1 g l^{-1} PMGly, unless noted otherwise). The concentrations of the substances contained in the calcification solutions are summarized in supplementary Tables 1–6.

Polymer film synthesis

First, 1 mg of the urease formulation was dissolved in $20 \mu\text{l}$ of the TEA buffer (concentration of 50 mg ml^{-1}).

For DMA-based networks: A mixture of 99 mg DMA and 1 mg TEG was prepared in a vessel. Optionally, up to 5 mg of the monomer was substituted with the additive monomer AA or EDPOA, respectively. Then, 0.5 mg of the photoinitiator Irgacure 651 and $20 \mu\text{l}$ of the urease solution were added to the mixture. The final compositions of the networks are summarized in supplementary Table 1.

For AAm-based conetworks: The monomer solution was prepared by dissolving AAm (500 g l^{-1}) in pure water. A mixture of 2 mg of the photoinitiator IG 2959, $6 \mu\text{l}$ of a MBAm solution (10 g l^{-1} in pure water) and the AAm solution was given to a vessel. Optionally, up to 100 mg of the monomer was substituted with the additive monomer SA. For every mg of additive monomer, $2 \mu\text{l}$ of degassed and bidistilled water was added to ensure solubility of SPA, DMAPS and SA. $20 \mu\text{l}$ of the urease solution was added to the mixture followed by vortexing. The final compositions of the networks are summarized in supplementary Tables 1–6.

The whole monomer–initiator–enzyme mixture was poured onto an adhesive-tape covered glass slide ($1 \times 3 \text{ inch}^2$) with distance holders of $300 \mu\text{m}$ and topped with another tape-covered slide. Polymerization was carried out in an ultraviolet light chamber (Emmi-Nail Premium at $\lambda = 340 \text{ nm}$ for 480 s (flipping the slide every 120 s)). Then, the glass slides were carefully separated, and the formed polymer film (thickness $300 \pm 30 \mu\text{m}$, $\sim 15 \times 30 \text{ mm}^2$) was calcified immediately.

Calcification

Two hundred milliliters of the tempered calcification solution (same temperature as subsequent calcification) was poured into a closed Schott glass bottle containing one urease-loaded network (polymer network to calcification solution ratio of 1 mg/1 ml). The immersed networks in the calcification solution were incubated at $20 \text{ }^\circ\text{C}$ in a climate chamber for 24 h, unless noted otherwise. The calcification temperature of 30 to $40 \text{ }^\circ\text{C}$ was controlled using a tempered oil bath. The resulting composite material was taken out after calcification and thoroughly rinsed with and stored in pure water at ambient temperature. The concentrations of the substances in the calcification solution, the compositions of the networks and the conditions during calcification are summarized in supplementary Tables 1–6.

Analytical methods

Calcified composite networks were broken in liquid nitrogen prior to analysis. The fracture surfaces of the cross sections were investigated by SEM. Samples were mounted on aluminum stubs with double-sided carbon tape and recorded using a Hitachi S-4500 SEM with field-emission gun and Oxford Link Isis-System. The acceleration voltage was set to 1 kV and the working distance to 8 mm. The modification of the inorganic phase was determined with a Bruker alpha ATR-FTIR spectrometer with absorption bands at $\sim 863 \text{ cm}^{-1}$ (ν_2), 1074 cm^{-1} (ν_1), 1386 cm^{-1} (ν_3) and 1474 cm^{-1} (ν_3) being typical for ACC, 742 cm^{-1} (ν_4), 874 cm^{-1} (ν_2) and 1405 cm^{-1} (ν_3) for vaterite, 714 cm^{-1} (ν_4), 852 cm^{-1} (ν_2) and 1447 cm^{-1} (ν_3) for aragonite and 712 cm^{-1} (ν_4), 873 cm^{-1} (ν_2) and 1393 cm^{-1} (ν_3) for calcite [48–50].

The inorganic proportion of the calcified composites was determined via thermal gravimetric analysis

(TGA; Netzsch STA 409 C) using sample sizes of 10–15 mg and a heating ramp of 10 °C/min up to 600 °C. To determine the inorganic proportion of ACC, the weight loss of the sample during pyrolysis was measured. Water evaporation occurred below 200 °C, while decomposition of organic content starts above this temperature. The difference between m_{dry} and $m_{combusted}$ was used to calculate the inorganic content m_{ACC} with $wt_{ACC} [\%] = m_{combusted} \times m_{dry}^{-1} \times 100$.

Stress–strain curves were recorded at ambient temperature using an Instron 3340 tensile tester with a cell with a load of 1 kN. Rectangular samples with dimensions of 5 × 20 mm (width × length) were cut using a razor blade. The thickness of each sample was individually measured (typically between 0.4 mm and 0.8 mm) and the samples mounted between the clamps with an initial distance of 10 mm. Sandpaper was used to prevent slippage of the samples between the grips. The experiment was performed at a cross-head speed of 5% min⁻¹ until the sample fractured, while the sample was permanently moistened with water using a spray can.

The fracture energy of a hydrated polymer network was determined as described with a method [51], which is used in the characterization of hydrogels [52]. At least three notched and three unnotched samples per composite (length 20 mm, width 5 mm, thickness 0.4–0.8 mm) were clamped in the Instron 3340 tensile tester (clamp-to-clamp distance 10 mm), and their stress–strain curves were measured with a crosshead speed of 5% min⁻¹. The notched samples were prepared by cutting a notch with a length of 50% of the sample width by using a razor blade (notch length 2.5 mm). These samples were used to determine the strain that is necessary to turn the notch into a running crack. The corresponding fracture energy (Γ in J m⁻²) of the unnotched samples is calculated as follows:

$$\Gamma = l_c \times \int_0^{\varepsilon_c} \sigma(\varepsilon) d\varepsilon$$

where σ is the stress (in MPa), ε is the strain (as a percentage), ε_c is the strain that results in fracture of notched samples (%) and l_c is the initial distance from clamp to clamp (in mm).

Swelling behavior

The mass of the dried (m_{dry}) and the swollen ($m_{swollen}$) composites or hydrogels was measured. Swelling

was performed in pure water at room temperature for 24 h. The swelling ratio is calculated with swelling ratio = $m_{swollen}/m_{dry}$.

Results and discussion

The objective of this work was to calcify hydrogels with calcium carbonate toward ultrastiff and tough organic–inorganic DN hydrogels. To this end, the inorganic CaCO₃ phase has to be precipitated as an amorphous and percolated structure, and the organic and the inorganic phases need to be connected by suited functional groups. The amorphous character of the CaCO₃ phase is realized by the previously reported method of the urease-induced mineralization in the presence of PMGly. The connection between the two phases is addressed by adding functional groups to the organic polymer network that can interact with calcium carbonate, e.g., phosphonate or carboxylate groups [33, 53, 54]. Thus, the following charged monomers were copolymerized with DMA and AAm, respectively, to achieve charged hydrogels that show enhanced stiffness after ACC precipitation: acrylic acid (AA) or ethyl 2-[4-(dihydroxyphosphoryl)-2-oxabutyl] acrylate (EDPOA) was used in PDMA-*l*-TEG networks. 2-Acrylamido-2-methylpropane sulfonic acid (AMPS), *N*-(3-Sulfopropyl)-*N*-(methacryloxyethyl)-*N*, *N*-dimethylammonium betaine (DMAPS), 2-methacryloyloxy ethyl trimethylammonium chloride (QuAAc), 3-Sulfopropyl acrylate potassium salt (SPA) and sodium acrylate (SA) were used in PAAm-*l*-MBAm networks, respectively (Fig. 1).

The ratio between the neutral and the charged monomers was continually changed until the degree of mineralization in the final DN hydrogel drops, i.e., the urease activity decreases. The mineralization was performed using the same chemical conditions as described earlier [47]. The calcification was performed at 20 °C for 24 h. The degrees of mineralization and Young's modulus of the organic–inorganic double-network hydrogels (O/I-DNHs) are provided in Supp. Tab. 1. Only PAAm-*l*-MBAm networks with carboxylate groups (SA as comonomer) afford mineralized hydrogels with strongly improved stiffness, while PDMA-*l*-TEG networks with EDPOA or AA do not undergo sufficient mineralization and PAAm-*l*-MBAm networks with AMPS, DMAPS, SPA and QuAAc do not experience any significant increase in

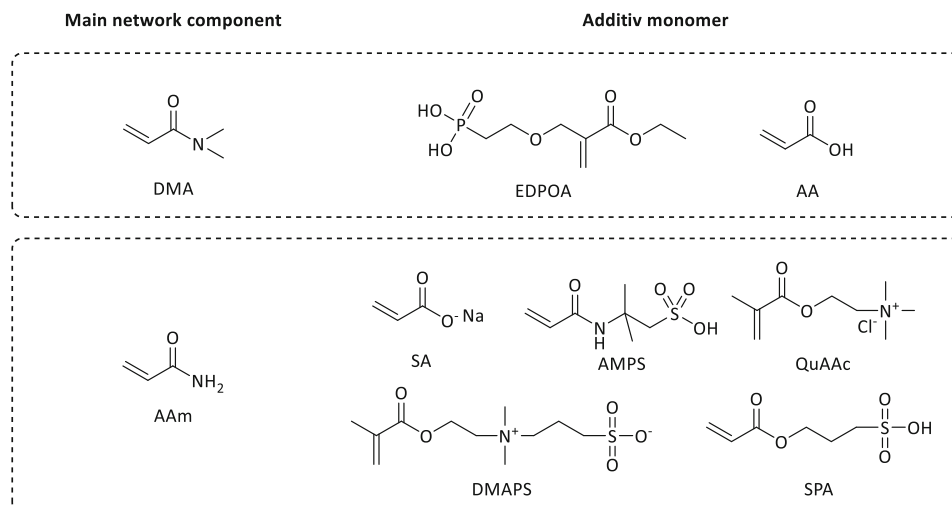


Figure 1 Monomers used for introducing charged functional groups into urease containing hydrogels. Acrylic acid (AA) or ethyl 2-[4-(dihydroxyphosphoryl)-2-oxabutyl] acrylate (EDPOA) was used in PDMA-*l*-TEG networks and *N*-(3-Sulfopropyl)-*N*-(methacryloyloxyethyl)-*N,N*-dimethylammonium betaine (DMAPS),

2-Acrylamido-2-methylpropane sulfonic acid (AMPS), 2-methacryloyloxy ethyl trimethylammonium chloride (QuAAc), 3-Sulfopropyl acrylate potassium salt (SPA) and sodium acrylate (SA) were used in PAAm-*l*-MBAm networks, respectively.

terms of stiffness. Figure 2a displays the degree of mineralization and the degree of swelling of PAAm-*l*-MBAm hydrogels with varying sodium acrylate content in the starting monomer mixture after mineralization at 20 °C for 24 h. The introduction of low amounts of SA of up to 10 wt.% leads to no higher degree of mineralization, but to an increased swelling ratio. This can be explained by the fact that the carboxylate ions increase the degree of swelling due to the electrostatic repulsion, and the interactions between ACC and organic network are only possible by very few ionic groups.

Further increase of the SA content leads to a decrease in swelling with no significant change of the inorganic content up to 50 wt.% SA. Hydrogels with an SA content of more than 50 wt.% SA show a decrease in inorganic content with the largest decrease for a mineralized material fully based on cross-linked SA. This behavior can be explained by an increasing binding strength between polymer matrix and ACC, which stands for higher cross-linking density, and a possibly decreased urease activity. The structure of the formed inorganic phase was investigated with SEM. As seen in Fig. 2b, the mineralized hydrogel without carboxylate groups is filled with spherical structures of some 200 nm in size. The addition of only 1 wt.% of the sodium acrylate monomer affords significantly smaller

spheres (76 ± 8 nm) as seen in Fig. 2c. The addition of higher amounts of the charged monomer up to 25 wt.% does not lead to different inorganic nanostructures. Increasing the acrylate content to 30 wt.% results in finer ACC structures, which partially form a continuous network (see Fig. 2d). Increasing the SA content to 35 wt.% leads to an even finer, more continuous inorganic network structure throughout the complete hydrogel (Supp. Figure 1), which also affords a higher optical transparency for visible light as seen in the photograph of Fig. 2e. A schematic representation of the mineralization process with and without carboxyl groups is shown in Fig. 3.

The degree of swelling for mineralized DN hydrogels with 20 to 40 wt.% SA is in a range of 2–2.5, which is typical for the best-performing comparable DN hydrogels with calcium phosphate. These materials were investigated regarding their mechanical performance as seen in Fig. 4, which compares the stiffness, the fracture energy, and the breaking strength of the water-swollen materials. While hydrogels with 20 and 25 wt.% SA show a moderate stiffness of 18 and 16 MPa, an increase in carboxylate content to 30 wt.% SA leads to a more than tenfold higher stiffness of around 200 MPa, which reaches up to 420 MPa for a 35 wt.% SA containing material. The highest stiffness of 466 MPa was found for the

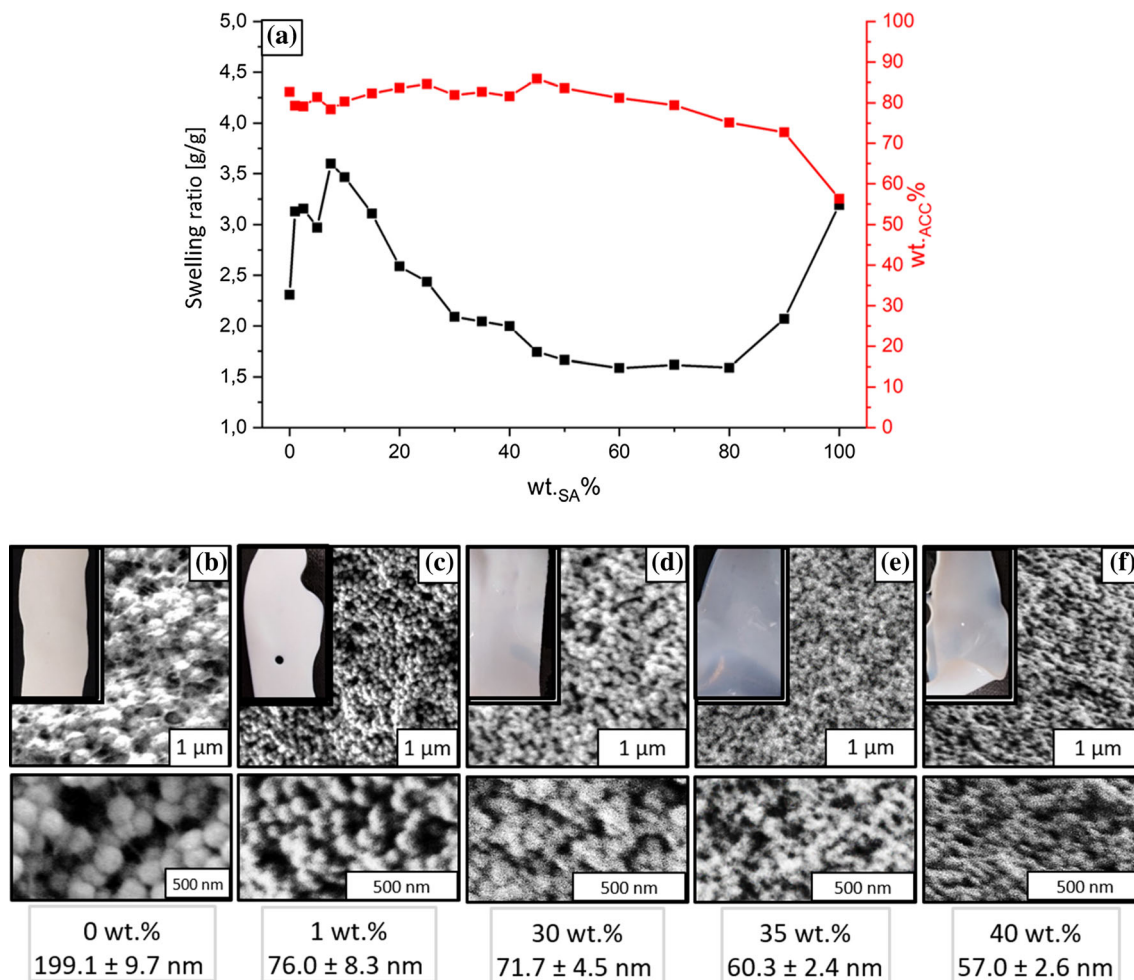


Figure 2 (a) Swelling ratio and degree of mineralization (wt. ACC%) of PAAm-*l*-MBAm networks (0.06 wt.% MBAm, 1 wt.% urease formulation (urease)) containing different amounts of sodium acrylate (0–100 wt.%) after calcification in an aqueous solution of CaCl₂ (30 g l⁻¹), urea (10 g l⁻¹) and PMGly (1 g l⁻¹) at 20 °C for 24 h (a). SEM images of PAAm-*l*-MBAm networks (0.06 wt.% MBAm, 1 wt.% urease formulation (urease))

containing different amounts of sodium acrylate (0, 1, 30, 35, 40 wt.%) after calcification in an aqueous solution of CaCl₂ (30 g l⁻¹), urea (10 g l⁻¹) and PMGly (1 g l⁻¹) at 20 °C for 24 h (b-f). The figure also shows images with higher resolution. Images were taken in the middle of the film. The figure further shows photographs of the respective calcified hydrogels in the top left corner of the SEM image.

hydrogel with 40 wt.% SA. A similar trend was found for the tensile strength.

The highest strengths of 2.9 and 3.1 MPa were found for ACC-mineralized hydrogels with 35 and 40 wt.% SA, respectively. The fracture energy increases to up to 800 J m⁻² (35 wt.% SA) with higher SA contents; however, the material becomes increasingly brittle when further increasing the SA content to 40 wt.%. Thus, the SA content clearly controls the mechanical properties of the ACC-mineralized hydrogels. Increasing amounts of SA do not influence the degree of mineralization up to 50 wt.%, but the materials become stiffer, stronger, and tougher with

higher SA content in the hydrogel. However, a SA content of 40 wt.% or higher results in very brittle materials. Obviously, the SA content of 35 wt.% is the optimal amount, where the best mechanical properties are achieved after mineralization. This is most likely due to the formation of an inorganic network within the hydrogel and the optimal binding between the organic and the inorganic networks. Higher SA contents still allow the formation of the inorganic network, but the binding between the organic and the inorganic phase becomes too strong and the organic phase cannot be used as sacrificial network anymore. Consequently, the degree of swelling decreases and

Figure 3 Schematic representation of the mineralization process with and without particle growth control, leading to different morphologies of the precipitated inorganic phase.

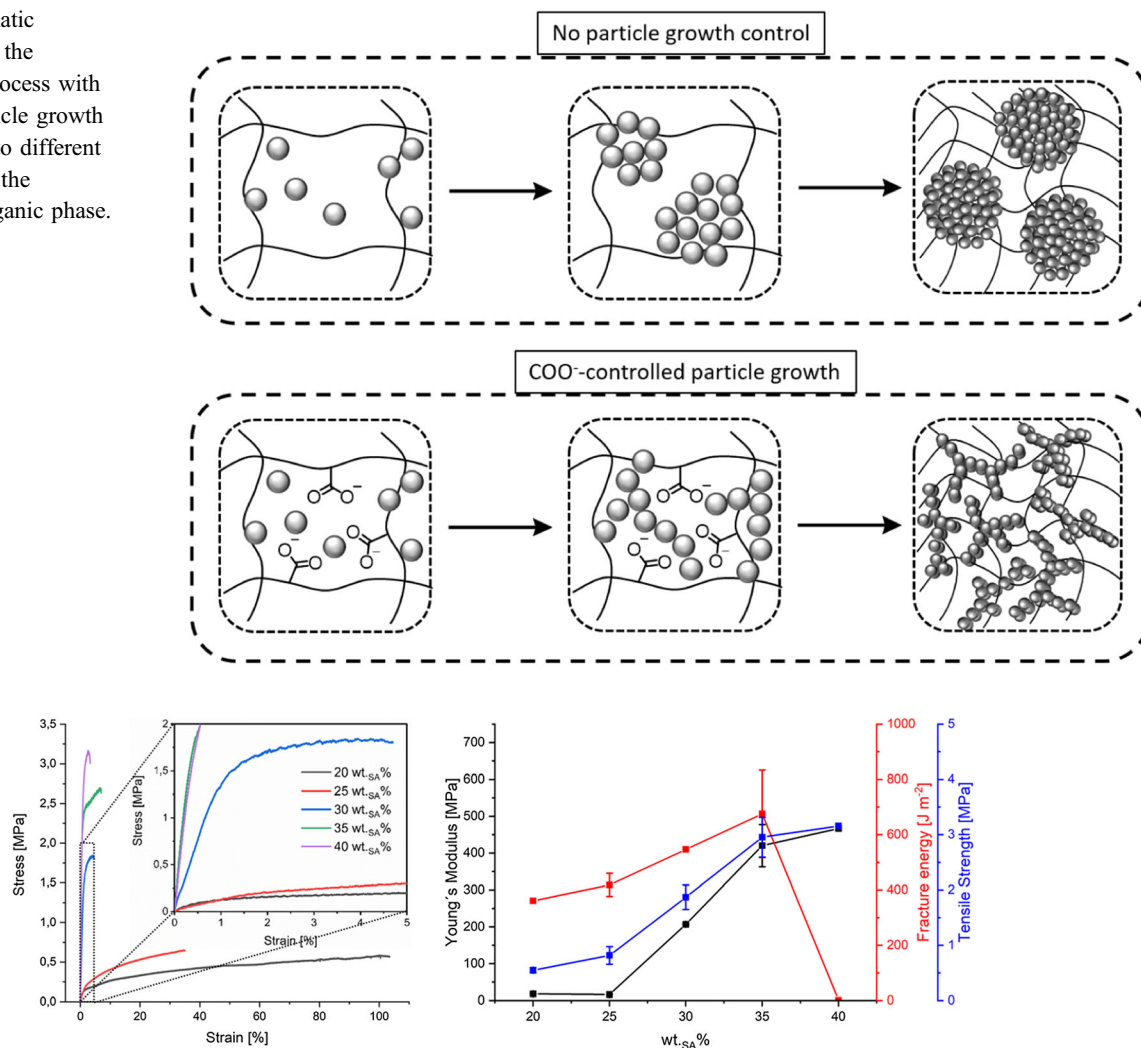


Figure 4 Stress–strain curves for PAAm-*l*-MBAm networks with 0.06 wt.% MBAm, 1 wt.% urease and 20–40 wt.% sodium acrylate after calcification in an aqueous solution of CaCl_2 (30 g l^{-1}), urea (10 g l^{-1}) and PMGly (1 g l^{-1}) at $20\text{ }^\circ\text{C}$ for 24 h (left diagram). Young's modulus (black), fracture energy

(red), and breaking stress (blue) of PAAm-*l*-MBAm networks with 0.06 wt.% MBAm, 1 wt.% urease and 20–40 wt.% sodium acrylate after calcification in an aqueous solution of CaCl_2 (30 g l^{-1}), urea (10 g l^{-1}) and PMGly (1 g l^{-1}) at $20\text{ }^\circ\text{C}$ for 24 h (right diagram).

the mechanical properties are dominated by the inorganic phase, rendering the material brittle.

The great increase in the stiffness of the organic–inorganic DN hydrogel has been explained by the percolation of the inorganic phase. Seemingly, there is an optimal structure, where the percolated inorganic phase carries the mechanical load, while the organic phase provides the toughness of the material. This is only possible at a point, where the inorganic phase does not yet form a massive and continuous stiff scaffold that permeates the material, but is still somewhat “imperfect” and thus flexible. In order to find this “sweet spot”, the kinetics of the ACC-

mineralization of the PAAm-*l*-MBAm with 35 wt._{SA}% was investigated. To this end, the hydrogel was given to the mineralization solution at $20\text{ }^\circ\text{C}$ and samples were taken at regular intervals and examined by SEM, thermogravimetric analysis, and tensile tests to get further insight in the formation and growth of the respective ACC phase during calcification. As seen in Fig. 5, the ACC content continuously increases for up to 16 h, where it reaches 76 wt._{ACC}%. After that, the inorganic weight content increases more slowly, reaching around 82 wt._{ACC}% after 24 h. The first significant improvement in mechanical properties is observed after 16 h of mineralization, when the

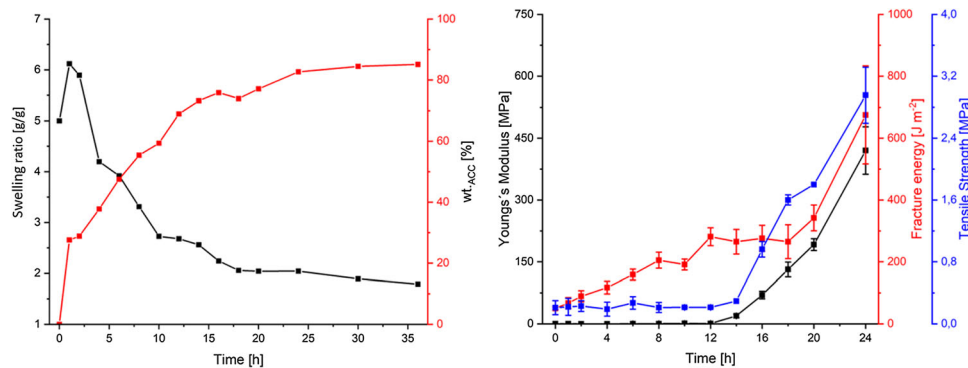


Figure 5 Swelling ratio and degree of mineralization (wt._{ACC}%) of PAAm-*l*-MBAm networks (0.06 wt.% MBAm, 1 wt.% urease formulation (urease)) containing 35 wt.% sodium acrylate after calcification in an aqueous solution of CaCl₂ (30 g l⁻¹), urea (10 g l⁻¹) and PMGly (1 g l⁻¹) at 20 °C for up to 24 h (left). Young's modulus, fracture energy and tensile breaking stress of

PAAm-*l*-MBAm networks (0.06 wt.% MBAm, 1 wt.% urease formulation (urease)) containing 35 wt.% sodium acrylate after calcification in an aqueous solution of CaCl₂ (30 g l⁻¹), urea (10 g l⁻¹) and PMGly (1 g l⁻¹) at 20 °C for up to 24 h (right diagram).

tensile strength increases from 0.2 (after 14 h) to 1.0 MPa. The first significant improvement in stiffness occurs after 14 h. Tensile strength and stiffness continuously improve, reaching a Young's Modulus of 420 MPa and a breaking strength of 3.0 MPa after 24 h. A further increase in the mineralization time beyond 24 h leads to severe embrittlement and thus unreliable mechanical measurements. Obviously, the percolation point is reached after a mineralization time of 14–16 h.

As shown previously, it is possible to greatly change mechanical properties before reaching the percolation point, when only slightly changing the degree of swelling. This was shown exemplary on PAAm-*l*-MBAm networks with 35 wt.% SA, 0.06 wt.% MBAm and 1 wt.% urease, which were mineralized for 8 h and 10 h, respectively. Both composites were slowly dried, and their Young's moduli were measured continuously. As seen in Fig. 6, the Young's modulus increases by a factor of 20 when the degree of swelling decreases from 2.4 to 2.1, reaching a seemingly critical threshold for networks after 8 h of calcification. The same can be observed for networks after a calcification time of 10 h, with the degree of swelling decreasing from 2.3 to 2.0. This jump can only be explained by percolation of the inorganic nanostructures according to a critical threshold in wt._{ACC}% and corresponds to the value observed during the investigation of the time-dependent calcification (cf. Figs. 5 and 6), leading to a percolated second network.

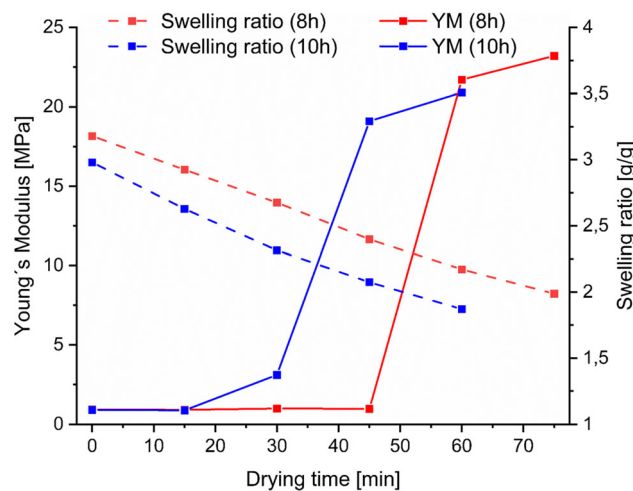


Figure 6 Measurements of Young's moduli (continuous lines) and the respective degrees of swelling (dashed lines) for PAAm-*l*-MBAm networks with 35 wt.% SA, 0.06 wt.% MBAm and 1 wt.% urease after 8 (red) and 10 (blue) hours of calcification at different stages of drying.

Altogether, the urease-induced mineralization of hydrogels with ACC results in composite materials with similar stiffness and toughness and a threefold higher tensile strength compared to the previously described alkaline phosphatase-based DN hydrogels. Due to the higher activity of urease, these properties are achieved within 24 h in contrast to 3 to 7 days, which are necessary for the alkaline phosphatase mineralization. Due to the higher temperature stability of urease (compared to the temperature-sensitive alkaline phosphatase), the mineralization process might be accelerated with increasing temperature. In

Figure 7 Swelling ratio and degree of mineralization **a**, **c** Young's modulus, fracture energy and tensile breaking stress **b**, **d** of PAAm-*l*-MBAm networks (0.06 wt.% MBAm, 1 wt.% urease formulation (urease)) containing 35 wt.% sodium acrylate after calcification in an aqueous solution of CaCl_2 (45 g l^{-1}), urea (15 g l^{-1}) and PMGly (1 g l^{-1}) at 35 (**a**, **b**) and 40 (**c**, **d**) °C for up to 8 h.

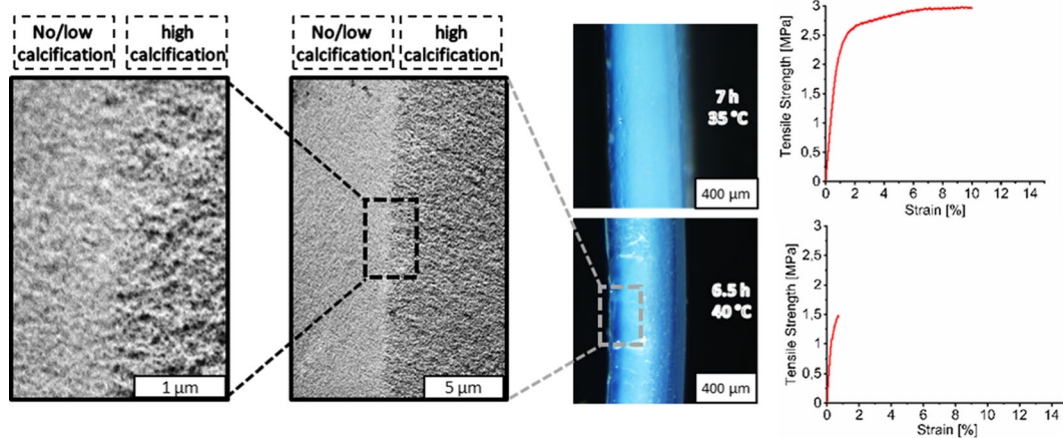
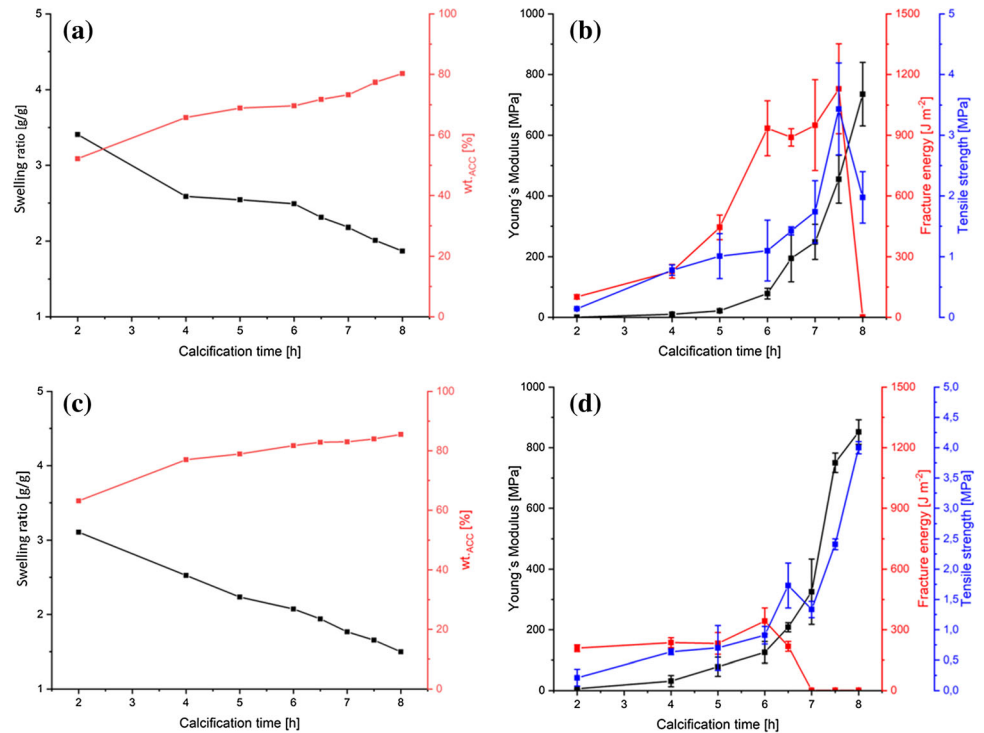


Figure 8 SEM images of cross-sections near the outer layer of PAAm-*l*-MBAm hydrogels mineralized for 6.5 h at 40 °C (left), stereomicroscope images of cross-sections of the same hydrogels mineralized for 7 h at 35 °C (middle top) and for 6.5 h at 40 °C (middle, bottom), and stress–strain curves of both mineralized

hydrogels (right top: mineralized for 7 h at 35 °C, right bottom: mineralized for 6.5 h at 40 °C). The PAAm-*l*-MBAm networks contained 0.06 wt.% MBAm, 1 wt.% urease and 35 wt.% sodium acrylate and were mineralized in an aqueous solution of CaCl_2 (45 g l^{-1}), urea (15 g l^{-1}) and PMGly (1 g l^{-1}) at 35 and 40 °C

order to find the percolation point for the highest stiffness and strength, while retaining high toughness, the mineralization was studied over time at 35 and 40 °C until maximum mechanical properties were achieved. As the substrate diffusion rate from the calcification solution into the hydrogel might be a

reaction-limiting factor, the substrate concentrations were increased to 45 g/L for CaCl_2 and 15 g/L for urea. As seen in Fig. 7a, the mineralization process at 35 °C is greatly accelerated, compared to the experiment at 20 °C. The percolation point for the optimal mechanical properties in terms of highest stiffness for

a still tough mineralized hydrogel is reached after 7.5 h (Fig. 7b), with a Young's modulus of 455 ± 80 MPa, a tensile strength of 3.4 ± 0.7 , and a breaking energy of 1.1 ± 0.2 kJ m⁻² with a critical strain of $13.0 \pm 3.5\%$. These properties are even superior to the previously reported calcium phosphate-mineralized hydrogels, particularly with respect to an almost tripled strength. Furthermore, the excellent mechanic characteristics are achieved in a more than tenfold shorter period of mineralization time. The strongly accelerated mineralization at higher temperatures suggests that the mineralization process is controlled by a chemical reaction, which is the urea hydrolysis.

Further increasing the reaction temperature to 40 °C leads to even faster mineralization, but without achieving the mechanical properties achieved at 35 °C (Fig. 7c, d). The composite hydrogel becomes significantly stiffer and stronger after 4 h and has a degree of calcification of nearly 80 wt.% after this time. However, the mineralized hydrogel is already brittle at this point. We presume that this is due to the reaction being diffusion controlled at this temperature. This leads to a depth-dependent and inhomogeneous mineralization, which generates a highly stiff and brittle layer inside the hydrogel, while layers near the surface appear to be soft (~ 15 μm, see Supp. Figure 4 for more detailed SEM-overview), because they are not yet mineralized, as SEM images of the respective mineralized hydrogel suggest (Fig. 8). Another explanation for the low toughness could be the formation of anisotropic calcite or aragonite crystals, which are known to make such a hydrogel brittle. This, however, was not the case, as the formation of a crystalline CaCO₃ structure could be excluded by respective FTIR measurements (Supp. Figure 5). Thus, depth-dependent inhomogeneous mineralization seems to be the reason for the observed mechanical properties. Increasing the CaCl₂ and urea concentration in the mineralization solution at 40 °C to 60 g l⁻¹ and 20 g l⁻¹, respectively, resulted in similar structures, while further increase to 75 and 25 g l⁻¹ yielded inhomogeneously mineralized hydrogels without any improvement in mechanical properties, due to a drop in enzyme activity, as lower inorganic wt._{ACC}% suggest (70 wt._{ACC}%). Thus, 35 °C seems to be the highest possible calcification temperature for homogenous mineralization of the here used hydrogels, with CaCl₂ and urea concentrations of 45 and 15 g l⁻¹.

Conclusion

The present work shows that the synthesis of organic–inorganic double network hydrogels based on amorphous inorganic minerals and organic hydrogel networks toward homogeneous, ultrastiff, strong and tough composite hydrogel networks is not limited to amorphous calcium phosphate and that enzyme-induced mineralization can be used as a general method to produce composite materials based on a variety of components. Further, the homogenous precipitation of percolating amorphous inorganic nanostructures massively improves the mechanical properties of the mineralized composites when compared to networks containing crystalline structures as a result of the isotropic nature of ACC.

The calcification process always shows a sudden increase in stiffness at a certain time point of mineralization. This point clearly indicates the percolation of the inorganic phase. The fast calcification process then leads to further mineralization, which eventually renders the material very brittle. Thus, the mechanical properties are mineralization time sensitive, and the process needs to be stopped at the right moment by removing the DN hydrogel from the mineralization solution and storing the material in water. This sharp percolation point is examined currently for its suitability for designing DN hydrogels with thermally switchable stiffness.

Another advantage of the urease-induced calcification is the robust enzyme, which allows mineralization even at higher temperatures to accelerate the process to 7.5 h at 35 °C. Higher temperatures of up to 60 °C are possible, but the process becomes diffusion controlled and leads to inhomogeneously mineralized materials. Thus, the 400–500 μm thick films prepared in this work cannot be mineralized faster, but this might not be true for smaller structures, such as enzyme-loaded microparticles [55, 56], fibers [57], or thin films [58], which might lead to new materials with interesting mechanical and optical properties. This will be addressed in future studies.

Acknowledgements

We thank Ivoclar Vivadent GmbH for providing EDPOA and Ciba Specialty Chemicals (part of BASF) for providing Irgacure 651.

Author Contributions

J.C.T. and M.M. designed the study and interpreted the results. M.M. and L.M. prepared the composites, performed TGA, FTIR, mechanic and swelling experiments and took optical and SEM images. V.B. performed TEM, SAED and EDX analysis. M.M. and L.M. established first bulk precipitation of percolating amorphous calcium carbonate with urease within hydrogels during the master thesis of L.M. at the TU Dortmund. M.M. and M.S. investigated time-dependent calcification during the bachelor thesis of M.S. J.C.T. and M.M. wrote the manuscript.

Funding

Open Access funding enabled and organized by Projekt DEAL.

Declarations

Conflict of interest The authors declare no competing financial interest.

Supplementary Information: The online version contains supplementary material available at <http://doi.org/10.1007/s10853-021-06204-6>.

Open Access This article is licensed under a Creative Commons Attribution 4.0 International License, which permits use, sharing, adaptation, distribution and reproduction in any medium or format, as long as you give appropriate credit to the original author(s) and the source, provide a link to the Creative Commons licence, and indicate if changes were made. The images or other third party material in this article are included in the article's Creative Commons licence, unless indicated otherwise in a credit line to the material. If material is not included in the article's Creative Commons licence and your intended use is not permitted by statutory regulation or exceeds the permitted use, you will need to obtain permission directly from the copyright holder. To view a copy of this licence, visit <http://creativecommons.org/licenses/by/4.0/>.

References

- [1] Mredha MTI, Kitamura N, Nonoyama T, Wada S, Goto K, Zhang X, Nakajima T, Kurokawa T, Takagi Y, Yasuda K, Gong JP (2017) Anisotropic tough double network hydrogel from fish collagen and its spontaneous in vivo bonding to bone. *Biomaterials* 132:85–95
- [2] Hoffman AS (2012) Hydrogels for biomedical applications. *Adv Drug Deliv Rev* 64:18–23
- [3] Slaughter BV, Khurshid SS, Fisher OZ, Khademhosseini A, Peppas NA (2009) Hydrogels in regenerative medicine. *Adv Mater* 21(32–33):3307–3329
- [4] Hunt JA, Chen R, van Veen T, Bryan N (2014) Hydrogels for tissue engineering and regenerative medicine. *J Mater Chem B* 2(33):5319–5338
- [5] Qiu Y, Park K (2001) Environment-sensitive hydrogels for drug delivery. *Adv Drug Deliv Rev* 53(3):321–339
- [6] Palleau E, Morales D, Dickey MD, Velev OD (2013) Reversible patterning and actuation of hydrogels by electrically assisted ionoprinting. *Nat Commun* 4(1):2257
- [7] Calvert P (2009) Hydrogels for Soft Machines. *Adv Mater* 21(7):743–756
- [8] Koetting MC, Peters JT, Steichen SD, Peppas NA (2015) Stimulus-responsive hydrogels: theory, modern advances, and applications. *Mater Sci Eng R Rep* 93:1–49
- [9] Kulkarni RV, Biswanath S (2007) Electrically responsive smart hydrogels in drug delivery: a review. *J Appl Biomater Biomech* 5(3):125–139
- [10] Yuk H, Lu B, Zhao X (2019) Hydrogel bioelectronics. *Chem Soc Rev* 48(6):1642–1667
- [11] Rong Q, Lei W, Liu M (2018) Conductive Hydrogels as Smart Materials for Flexible Electronic Devices. *Chem–Eur J* 24(64):16930–16943
- [12] Kamoun EA, Kenawy E-RS, Chen X (2017) A review on polymeric hydrogel membranes for wound dressing applications: PVA-based hydrogel dressings. *J Adv Res* 8(3):217–233
- [13] Anis SF, Hashaikeh R, Hilal N (2019) Functional materials in desalination: a review. *Desalination* 468:114077
- [14] Daer S, Kharraz J, Giwa A, Hasan SW (2015) Recent applications of nanomaterials in water desalination: a critical review and future opportunities. *Desalination* 367:37–48
- [15] Shalla A, Yaseen Z, Bhat M, Ahmad T, Maswal M (2018) Recent review for removal of metal ions by hydrogels. *Sep Sci Technol* 54:1–12
- [16] Zhong L, Wang T, Liu L, Du W, Wang S (2018) Ultra-fine SiO₂ nanofilament-based PMIA: a double network membrane for efficient filtration of PM particles. *Sep Purif Technol* 202:357–64

- [17] Chu YY, Song XF, Zhao HX (2019) Water-swella-ble, tough, and stretchable inorganic–organic sulfoaluminate cement/polyacrylamide double-network hydrogel composites. *J Appl Polym Sci* 136(35):47905
- [18] Li X, Yang Q, Zhao Y, Long S, Zheng J (2017) Dual physically crosslinked double network hydrogels with high toughness and self-healing properties. *Soft Matter* 13(5):911–920
- [19] Sittko I, Kremser K, Roth M, Kuehne S, Stuhr S, Tiller JC (2015) Amphiphilic polymer conetworks with defined nanostructure and tailored swelling behavior for exploring the activation of an entrapped lipase in organic solvents. *Polymer* 64:122–129
- [20] Tobis J, Boch L, Thomann Y, Tiller JC (2011) Amphiphilic polymer conetworks as chiral separation membranes. *J Membr Sci* 372(1):219–227
- [21] Tobis J, Thomann Y, Tiller JC (2010) Synthesis and characterization of chiral and thermo responsive amphiphilic conetworks. *Polymer* 51(1):35–45
- [22] Dech S, Wruk V, Fik CP, Tiller JC (2012) Amphiphilic polymer conetworks derived from aqueous solutions for biocatalysis in organic solvents. *Polymer* 53(3):701–707
- [23] Bruns N, Bannwarth W, Tiller JC (2008) Amphiphilic conetworks as activating carriers for the enhancement of enzymatic activity in supercritical CO₂. *Biotechnol Bioeng* 101(1):19–26
- [24] Hanko M, Bruns N, Tiller JC, Heinze J (2006) Optical biochemical sensor for determining hydroperoxides in non-polar organic liquids as archetype for sensors consisting of amphiphilic conetworks as immobilisation matrices. *Anal Bioanal Chem* 386(5):1273–1283
- [25] Krumm C, Konieczny S, Dropalla GJ, Milbradt M, Tiller JC (2013) Amphiphilic polymer conetworks based on end group cross-linked poly(2-oxazoline) homo- and triblock copolymers. *Macromolecules* 46(9):3234–3245
- [26] Okumura Y, Ito K (2001) The Polyrotaxane Gel: A Topological Gel by Figure-of-Eight Cross-links. *Adv Mater* 13(7):485–487
- [27] Chen Q, Chen H, Zhu L, Zheng J (2015) Fundamentals of double network hydrogels. *J Mater Chem B* 3(18):3654–3676
- [28] Gong JP (2010) Why are double network hydrogels so tough? *Soft Matter* 6(12):2583–2590
- [29] Gong JP, Katsuyama Y, Kurokawa T, Osada Y (2003) Double-network hydrogels with extremely high mechanical strength. *Adv Mater* 15(14):1155–1158
- [30] Strassburg A, Petranowitsch J, Paetzold F, Krumm C, Peter E, Meuris M, Köller M, Tiller JC (2017) Cross-linking of a hydrophilic, antimicrobial polycation toward a fast-swelling, antimicrobial superabsorber and interpenetrating hydrogel networks with long lasting antimicrobial properties. *ACS Appl Mater Interfaces* 9(42):36573–36582
- [31] Rauner N, Buenger L, Schuller S, Tiller JC (2015) Post-polymerization of urease-induced calcified, polymer hydrogels. *Macromol Rapid Commun* 36(2):224–230
- [32] Rauner N, Meuris M, Dech S, Godde J, Tiller JC (2014) Urease-induced calcification of segmented polymer hydrogels – a step towards artificial biomineralization. *Acta Biomater* 10(9):3942–3951
- [33] Rauner N, Meuris M, Zoric M, Tiller JC (2017) Enzymatic mineralization generates ultrastiff and tough hydrogels with tunable mechanics. *Nature* 543:407
- [34] Martin N, Youssef G (2018) Dynamic properties of hydrogels and fiber-reinforced hydrogels. *J Mech Behav Biomed Mater* 85:194–200
- [35] Jordan AM, Kim S-E, Van de Voorde K, Pokorski JK, Korley LTJ (2017) In situ fabrication of fiber reinforced three-dimensional hydrogel tissue engineering scaffolds. *ACS Biomater Sci Eng* 3(8):1869–1879
- [36] Agrawal A, Rahbar N, Calvert PD (2013) Strong fiber-reinforced hydrogel. *Acta Biomater* 9(2):5313–5318
- [37] Fukao K, Tanaka K, Kiyama R, Nonoyama T, Gong JP (2020) Hydrogels toughened by biominerals providing energy-dissipative sacrificial bonds. *J Mater Chem B* 8(24):5184–5188
- [38] Gao G, Du G, Cheng Y, Fu J (2014) Tough nanocomposite double network hydrogels reinforced with clay nanorods through covalent bonding and reversible chain adsorption. *J Mater Chem B* 2(11):1539–1548
- [39] Han IK, Chung T, Han J, Kim YS (2019) Nanocomposite hydrogel actuators hybridized with various dimensional nanomaterials for stimuli responsiveness enhancement. *Nano Convergence* 6(1):18
- [40] Haraguchi K, Li H-J (2006) Mechanical properties and structure of polymer–clay nanocomposite gels with high clay content. *Macromolecules* 39(5):1898–1905
- [41] Wang Q, Hou R, Cheng Y, Fu J (2012) Super-tough double-network hydrogels reinforced by covalently compositing with silica-nanoparticles. *Soft Matter* 8(22):6048–6056
- [42] Yu L, Wang D, Tan Y, Du J, Xiao Z, Wu R, Xu S, Huang J (2018) Super tough bentonite/SiO₂-based dual nanocomposite hydrogels using silane as both an intercalator and a crosslinker. *Appl Clay Sci* 156:53–60
- [43] Takafuji M, Alam MA, Goto H, Ihara H (2015) Microspherical hydrogel particles based on silica nanoparticle-webbed polymer networks. *J Colloid Interface Sci* 455:32–38
- [44] Thoniyot P, Tan MJ, Karim AA, Young DJ, Loh XJ (2015) Nanoparticle-hydrogel composites: concept, design, and

- applications of these promising, multi-functional materials. *Adv Sci* 2(1–2):1400010
- [45] Liu Q, Nian G, Yang C, Qu S, Suo Z (2018) Bonding dissimilar polymer networks in various manufacturing processes. *Nat Commun* 9(1):846
- [46] Yasui T, Kamio E, Matsuyama H (2018) Inorganic/organic double-network ion gels with partially developed silica-particle network. *Langmuir* 34(36):10622–10633
- [47] Milovanovic M, Unruh MT, Brandt V, Tiller JC (2020) Forming amorphous calcium carbonate within hydrogels by enzyme-induced mineralization in the presence of N-(phosphonomethyl)glycine. *J Colloid Interface Sci* 579:357–368
- [48] Sun S, Mao L-B, Lei Z, Yu S-H, Cölfen H (2016) Hydrogels from amorphous calcium carbonate and polyacrylic acid: bio-inspired materials for “Mineral Plastics.” *Angew Chem Int Ed* 55(39):11765–11769
- [49] Nebel H, Neumann M, Mayer C, Epple M (2008) On the structure of amorphous calcium carbonate—a detailed study by solid-state NMR spectroscopy. *Inorg Chem* 47(17):7874–7879
- [50] Reeder RJ, Tang Y, Schmidt MP, Kubista LM, Cowan DF, Phillips BL (2013) Characterization of structure in biogenic amorphous calcium carbonate: pair distribution function and nuclear magnetic resonance studies of lobster gastrolith. *Cryst Growth Des* 13(5):1905–1914
- [51] Rivlin RS, Thomas AG (1953) Rupture of rubber. I. Characteristic energy for tearing. *J Poly Sci* 10(3):291–318
- [52] Sun JY, Zhao X, Illeperuma WR, Chaudhuri O, Oh KH, Mooney DJ, Vlassak JJ, Suo Z (2012) Highly stretchable and tough hydrogels. *Nature* 489(7414):133–136
- [53] Gkioni K, Leeuwenburgh SC, Douglas TE, Mikos AG, Jansen JA (2010) Mineralization of hydrogels for bone regeneration. *Tissue Eng Part B Rev* 16(6):577–85
- [54] Schweizer S, Taubert A (2007) Polymer-controlled, bio-inspired calcium phosphate mineralization from aqueous solution. *Macromol Biosci* 7(9–10):1085–1099
- [55] Savin G, Bruns N, Thomann Y, Tiller JC (2005) Nanophase separated amphiphilic microbeads. *Macromolecules* 38(18):7536–7539
- [56] Schoenfeld I, Dech S, Ryabenky B, Daniel B, Glowacki B, Ladisch R, Tiller JC (2013) Investigations on diffusion limitations of biocatalyzed reactions in amphiphilic polymer conetworks in organic solvents. *Biotechnol Bioeng* 110(9):2333–2342
- [57] Plothe R, Sittko I, Lanfer F, Fortmann M, Roth M, Kolbach V, Tiller JC (2017) Poly(2-ethylloxazoline) as matrix for highly active electrospun enzymes in organic solvents. *Biotechnol Bioeng* 114(1):39–45
- [58] Dech S, Cramer T, Ladisch R, Bruns N, Tiller JC (2011) Solid-solid interface adsorption of proteins and enzymes in nanophase-separated amphiphilic conetworks. *Biomacromol* 12(5):1594–1601

Publisher's Note Springer Nature remains neutral with regard to jurisdictional claims in published maps and institutional affiliations.